

PCCP

Accepted Manuscript



This is an *Accepted Manuscript*, which has been through the Royal Society of Chemistry peer review process and has been accepted for publication.

Accepted Manuscripts are published online shortly after acceptance, before technical editing, formatting and proof reading. Using this free service, authors can make their results available to the community, in citable form, before we publish the edited article. We will replace this *Accepted Manuscript* with the edited and formatted *Advance Article* as soon as it is available.

You can find more information about *Accepted Manuscripts* in the [Information for Authors](#).

Please note that technical editing may introduce minor changes to the text and/or graphics, which may alter content. The journal's standard [Terms & Conditions](#) and the [Ethical guidelines](#) still apply. In no event shall the Royal Society of Chemistry be held responsible for any errors or omissions in this *Accepted Manuscript* or any consequences arising from the use of any information it contains.

p/n-Polarity of thiophene oligomers in photovoltaic cells: Role of molecular vs supramolecular properties

Cite this: DOI: 10.1039/x0xx00000x

Tanwistha Ghosh,^{a,c} Anesh Gopal,^b Akinori Saeki,^{*b} Shu Seki^b and Vijayakumar C. Nair,^{*a,c}

Received 00th January 2012,
Accepted 00th January 2012

DOI: 10.1039/x0xx00000x

www.rsc.org/

Molecular and supramolecular properties play key roles on the optoelectronic properties and photovoltaic performances of organic materials. In the present work, we show how a small change in the molecular structure affects such properties, which in turn control the intrinsic and fundamental property such as the p/n-polarity of organic semiconductors in bulk-heterojunction solar cells. Herein, we designed and synthesized two acceptor-donor-acceptor type semiconducting thiophene oligomers end-functionalized with oxazolone/isoxazolone derivatives (**OT1** and **OT2** respectively). The HOMO - LUMO energy levels of both derivatives were found to be positioned in such a way that they can act as electron acceptors to P3HT and electron donors to PCBM. However, **OT1** functions as a donor (with PCBM) and **OT2** as an acceptor (with P3HT) in BHJ photovoltaic cells, and the reverse roles either results no or poor performance of the cell. Detailed studies using UV-vis absorption and fluorescence spectroscopy, time-correlated single photon counting, UV-photoelectron spectroscopy, density functional theory calculations, X-ray diffraction, and thermal gravimetric analysis proved that both molecular and supramolecular properties were contributing equally but in a contrasting manner to the above mentioned observation. The obtained results were further validated by flash-photolysis time-resolved microwave conductivity studies which showed excellent correlation between the structure, property, and device performances of the materials.

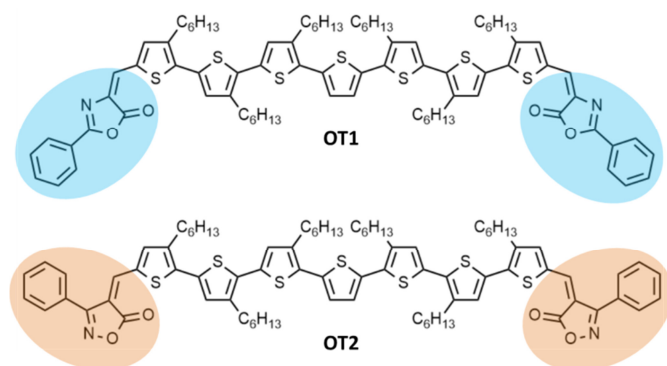
Introduction

Organic solar cells have attracted significant scientific interest because of their easy fabrication using low cost solution processing techniques, and compatibility with light weight, large area, flexible substrates.¹⁻⁵ Bulk-heterojunction (BHJ) is the most commonly used device configuration for organic solar cells, which consists of interpenetrating, bi-continuous networks of donor and acceptor, and offers maximum internal interfacial area for efficient charge separation.⁶⁻⁸ Thiophene-based polymers and fullerene-based small molecules are typical examples for donors and acceptors, respectively used in organic solar cells.⁹⁻¹² It is well established that molecular properties of polymers such as absorption characteristics, the highest occupied molecular orbital (HOMO) and the lowest unoccupied molecular orbital (LUMO) energy levels etc. play important roles on the device performances. Such properties could be easily controlled by suitable structural changes to the conjugated backbone.¹³⁻¹⁷ In addition to the molecular properties, supramolecular interactions among and between donor polymers and fullerene acceptors also play key role on the functionality and device performances of a bulk-heterojunction assembly.¹⁸⁻²¹ Rational choice of solvents, solvent additives and processing conditions were found to affect the supramolecular interactions, and hence the optoelectronic properties and device performances significantly.²²⁻²⁷ In this context, we have reported the switching of

charge carrier transport properties (from n-type to ambipolar) of a bithiazole-benzothiadiazole-based polymer through supramolecular control over structural organization induced by a solvent additive.²⁸ Furthermore, the 12 fold enhancement of charge carrier mobility was demonstrated for the same polymer through the self-assembly on gold nanoparticles.²⁹

Recently, small molecule/oligomer based organic semiconductors gained importance over their polymer counterparts for photovoltaic applications.³⁰⁻³⁵ When compared to polymers, oligomers are relatively easy to synthesize in high purity, possess well-defined structures, and show no batch-to-batch variations. Moreover, recent reports suggest that a promising power conversion efficiency (PCE) of ~10 % have been achieved in solution processed small molecules.³⁶⁻³⁸ Due to these advantages and recent findings, oligomers are now considered as a potential replacement for polymers in solution processed organic solar cells. However, dependence on supramolecular interactions is more pronounced in oligomers when compared to that of polymers, which demands careful molecular designing and rational fabrication techniques for obtaining optimum performances. This effect could be attributed to the limited pathways available for oligomers for charge transport; unlike polymers, where inter- and intra-polymer routes are available for charge transport,³⁹⁻⁴⁰ oligomers depends exclusively on intermolecular routes. This may result in significant variations in optoelectronic properties of comparable oligomers even when the structural differences

between them are minimal. In this context, Yagai *et al.* have reported the effect of regioisomerism on the optoelectronic properties of hydrogen bonding naphthalene chromophores.⁴¹ The same group has reported similar effect on the solid state properties and bulk heterojunction solar cell performance of indolocarbazoles end-capped with diketopyrrolopyrroles also.⁴² Herein, we report an excellent example illustrating the effect of small structural changes on the molecular and supramolecular properties of conjugated oligomers, which in turn affect their p/n-polarity and photovoltaic performance in a bulk-heterojunction solar cell. We have designed and synthesized two thiophene oligomers consisting of seven thiophene rings connected each other at 2,5-positions, and end-functionalized with oxazolone (OT1) or isoxazolone (OT2) derivatives (Scheme 1). Oxazolone and isoxazolone are positional isomers which differ in the respective positions of nitrogen atom and phenyl group on the 5-membered heterocyclic ring. Both of them are good electron acceptors because of the presence of electronegative heteroatoms and electron withdrawing carbonyl group in conjugation. All thiophenes in OT1 and OT2, except the middle one is attached with *n*-hexyl chains for solution processability.



Scheme 1. Chemical structure of the thiophene oligomers under study.

Experimental

Materials

All chemicals for synthesis were purchased either from local suppliers or from Aldrich, Alfa Aesar, or TCI. Air- and water-sensitive synthetic steps were performed in argon atmosphere using standard Schlenk techniques. Poly(3,4-ethylenedioxythiophene):poly(styrene sulfonate) (PEDOT:PSS) (Baytron P VP AI 4083) and Indium Tin Oxide (ITO)-coated glass substrates ($< 15 \Omega \text{ square}^{-1}$) were purchased from H. C. Stark and Sanyo Shinku Corp., respectively. [6,6]-Phenyl-C₆₁-butyric acid methyl ester (PCBM) and regio-regular poly(3-hexylthiophene-2,5-diyl) (P3HT) were purchased from Frontier Carbon Inc. and Aldrich respectively.

Measurements

Melting points were determined with a Mel-Temp-II melting point apparatus and are uncorrected. ¹H and ¹³C NMR spectra were recorded on 600 MHz Bruker Avance DRX-600 Spectrometer and DPX 500 MHz spectrometer. All the chemical shifts were referenced to (CH₃)₄Si (TMS; $\delta = 0$ ppm) for ¹H or residual CHCl₃ ($\delta = 77$ ppm) for ¹³C. High-resolution LCMS-TOF and MALDI-TOF mass spectra were obtained with KRATOS ANALYTICAL SHIMADZU

mass spectrometer using α -cyano-4-hydroxy cinnamic acid as the matrix.

Absorption and Fluorescence Spectroscopy: Electronic absorption spectra were recorded on a Shimadzu UV-3101 spectrophotometer using quartz cuvettes with 1 cm path length. Fluorescence spectra were collected using Fluorolog HORIBA JOBINYVON.

Fluorescence Quantum Yield and Lifetime: Fluorescence quantum yields were determined relative to standard compounds (rhodamine B in ethanol; $\phi_F = 0.5$) using optically matching solutions. Fluorescence lifetimes were measured using an IBH FluoroCube time correlated picosecond single photon counting (TCSPC) system. Samples were excited using a pulsed diode laser (< 100 ps pulse duration) at a wavelength of 375 nm (NanoLED-11) with a repetition rate of 1 MHz.

UV Photoelectron Yield Spectroscopy (PYS): PYS measurements were performed on a Sumitomo Heavy Industry Co. PCR-202. For this measurement, thin films of the oligomers were spin-casted on an ITO-coated glass surface from chlorobenzene solution. The solvent was completely removed under vacuum before mounting on to the spectrometer. Photoelectrons emitted from the films were detected after illuminating the film with UV radiation. With photon energy increased with an interval of 0.1 eV, the photoelectron counts were measured.

Density Functional Theory (DFT): For obtaining energy minimized structures of the molecules, DFT calculations were performed using Gaussian 09.⁴³ The B3LYP functions with the 6-31G(d,p) basis set were used. For simplicity, the *n*-hexyl side chains were replaced by methyl groups.

X-Ray Diffraction: XRD analysis done by using a Xeuss Simultaneous WAXs using Ni-filtered Cu K α radiation ($\lambda = 0.15405$ nm).

Thermogravimetry: Thermal gravimetric analysis was carried out by the use of Perkin Elmer STA 6000 simultaneous thermal analyzer. Platinum pans were used for the measurement and as the reference sample. The analysis was conducted between 50 and 600 °C at 10 °C min⁻¹ under dry N₂.

Flash-Photolysis Time-Resolved Microwave Conductivity (FP-TRMC):⁴⁴ Transient conductivity was measured by FP-TRMC technique. A resonant cavity was used to obtain a high degree of sensitivity in the measurement. The resonant frequency and the microwave power were set at ~ 9.1 GHz and 3 mW, respectively, so that the electric field of the microwave was sufficiently small not to disturb the motion of charge carriers. The value of conductivity is converted to the product of the quantum yield (ϕ) and the sum of charge carrier mobilities ($\Sigma\mu$), by the following equation.

$$\phi \Sigma \mu = \frac{1}{e \cdot A \cdot I_0 \cdot F_{\text{light}}} \cdot \frac{\Delta P_r}{P_r} \quad (1)$$

where e , A , I_0 , F_{light} , ΔP_r , and P_r are the unit charge of a single electron, a sensitivity factor [$(\text{S/m})^{-1}$], incident photon density of excitation laser (photons/m²), a correction (or filling) factor ($/\text{m}$), a change of reflected microwave power, and a power of reflected microwave, respectively. The change of conductivity is equivalent with $\Delta P_r / (A P_r)$. 500 nm laser light with a photon density of 6.4×10^{15} photons/cm² was used as the excitation source. The sample was set at the highest electric field in a resonant cavity. The experiments were carried out at room temperature.

Photovoltaic Device Fabrication. The ITO coated glass was first cleaned by ultra-sonication with a series of solvents from diluted detergent, water, acetone and isopropyl alcohol, dried under air stream and UV/ozone treated for 20 min. A ZnO layer was deposited on ITO surface by using a reported sol-gel method (0.1 g/ml zinc

acetate dihydrate and 0.028 g/ml ethanolamine in 2-methoxyethanol). The ZnO solution was spin-coated and annealed at 200 °C for 30 min. A hot solution (80 °C) of oligomer and PCBM or P3HT mixture was spin-coated on top of the ZnO layer from different solvents in a nitrogen atmosphere at 25 °C. The thickness of the active layer was controlled by rotation speed and measured by a surface profiler (ULVAC model Dektak 150). After spin coating, the photoactive layer was transferred to ultra-high vacuum chamber and waited at least for 30 min to remove residual solvent additive. On top of the active layer 10 nm MoO_x and 100 nm Ag layers were sequentially deposited using a shadow mask by thermal evaporation. The final device configuration was ITO (120-160 nm)/ZnO (30 nm)/BHJ active layer /MoO_x (10 nm)/Ag (100 nm) with an active area of 7.1 mm². Current-voltage (*J-V*) curves were measured using a source-measure unit (ADCMT Corp., 6241A) under AM 1.5 G solar illumination at 100 mW cm⁻² (1 sun, monitored by a calibrated standard cell, Bunko Keiki SM-250KD) from a 300 W solar simulator (SAN-EI Corp., XES-301S). The EQE spectra were measured by a Bunko Keiki model BS-520BK equipped with a Keithley model 2401 source meter. The monochromatic light power was calibrated by a silicon photovoltaic cell, Bunko Keiki model S1337-1010BQ.

Synthesis and Characterization

General procedure for Suzuki coupling: Dibromothiophene derivative and 3-hexylthiophene-2-boronic acid pinacol ester were weighed to a two necked flask and dissolved in deoxidized toluene. 2M aq. K₂CO₃ and a few drops of Aliquat 336 were added to the mixture and the flask was equipped with a reflux condenser and septum. Air was removed from the setup and replaced by Ar for three times by using freeze-pump-thaw method, then Pd(PPh₃)₄ was added under Ar counter flow. The reaction mixture was heated and stirred under Ar for 24 hours, then poured into water and extracted with CH₂Cl₂. The combined organic layers were washed with brine and water, dried over Na₂SO₄ and evaporated to dryness under vacuum.

General procedure for bromination:⁴⁵ Thiophene derivative was dissolved in chloroform-acetic acid mixture (1:1 v/v). The reaction mixture was kept in the dark and cooled to 0 °C by using salt-ice bath. *N*-Bromosuccinimide was added in several portions, and the reaction mixture was stirred at room temperature for 6 h followed by stirring at 50 °C for 4 hours. The reaction mixture was then added to water and extracted with CH₂Cl₂. The combined organic layers were washed with aq. NaHCO₃, brine and water, dried over Na₂SO₄ and evaporated to dryness under vacuum.

2.3.1. Synthesis of 3,3'-dihexyl-2,2':5,2''-terthiophene (1): **1** was prepared by Suzuki coupling using 2,5-dibromothiophene (3.20 g, 13.23 mmol, 1 equiv.), 3-hexylthiophene-2-boronic acid pinacol ester (8.17 g, 27.78 mmol, 2.1 equiv.), 2M aq. K₂CO₃ (30 mL), Aliquat 336 (4 drops), Pd(PPh₃)₄ (0.92 g, 0.79 mmol, 0.06 equiv.) and toluene (100 mL). The crude product was purified by column chromatography (silica gel, hexane) to provide **1** as a viscous pale yellow liquid. Yield: 74%; δ_H (600 MHz, CDCl₃, ppm) 7.20 (d, 2H, *J* = 5.4 Hz), 7.08 (s, 2H), 6.96 (d, 2H, *J* = 5.4 Hz), 2.80 (t, 4H, *J* = 7.8 Hz), 1.63-1.68 (m, 4H), 1.22-1.35 (m, 12H), 0.87 (t, 6H, *J* = 7 Hz); δ_C (150 MHz, CDCl₃, ppm) 139.69, 136.07, 130.27, 126.07, 123.72, 31.73, 30.78, 29.31, 29.25, 22.64, 14.12.

2.3.2. Synthesis of 5,5''-dibromo-3,3''-dihexyl-2,2':5',2''-terthiophene (2): Bromination of terthiophene **1** (2.00 g, 4.80 mmol, 1.0 equiv.) was carried out using *N*-bromosuccinimide (1.79 g, 10.08 mmol, 2.1 equiv.), in chloroform - acetic acid mixture (100 mL). The crude product was purified by column chromatography (silica gel, 50% CHCl₃-hexane). Pure product was obtained as light yellow oil.

Yield: 98%; δ_H (600 MHz, CDCl₃, ppm): 6.97 (s, 2H), 6.89 (s, 2H), 2.69 (t, *J* = 7.8, 4H), 1.65-1.54 (m, 4H), 1.29-1.27 (m, 12H), 0.87 (t, *J* = 3.6, 6H); δ_C (150 MHz, CDCl₃, ppm): 140.47, 135.15, 132.68, 131.57, 126.44, 110.65, 31.59, 30.55, 29.20, 29.11, 22.62, 14.09.

2.3.2. Synthesis of 3,3',3''',3''''-quadrithexyl-2,5':2',5''-2'',2''':5''',2''''-quinquethiophene (3): **3** was synthesized through Suzuki coupling using dibromoterthiophene **2** (1.90 g, 3.31 mmol, 1.0 equiv.), 3-hexylthiophene-2-boronic acid pinacol ester (2.04 g, 6.95 mmol, 2.1 equiv.), 2M aq. K₂CO₃ (16.5 mL), Aliquat 336 (2 drops), Pd(PPh₃)₄ (191 mg, 0.17 mmol, 0.05 equiv.), and toluene (30 mL). The crude product was purified using column chromatography (silica gel, hexane). Pure product was obtained as viscous golden yellow oil. Yield: 83%; δ_H (600 MHz, CDCl₃, ppm): 7.16 (d, *J* = 4.8, 2H), 7.08 (s, 2H), 6.95 (s, 2H), 6.93 (d, *J* = 4.8, 2H), 2.78 (t, *J* = 9.6, 8H), 1.70-1.63 (m, 8H), 1.37-1.29 (m, 24H), 0.88 (m, 12H); δ_C (150 MHz, CDCl₃, ppm): 139.85, 139.65, 135.72, 134.24, 130.44, 130.22, 130.09, 128.74, 125.89, 123.61, 31.68, 31.66, 30.65, 30.58, 29.44, 29.28, 29.26, 29.21, 22.63, 22.62, 14.09.

2.3.3. Synthesis of 5,5''''-dibromo-3,3',3''',3''''-quadrithexyl-2,5':2',5''-2'',2''':5''',2''''-quinquethiophene (4): **3** (1.20 g, 1.60 mmol, 1.0 equiv.) was brominated using *N*-bromosuccinimide (0.60 g, 3.36 mmol, 2.1 equiv.), in chloroform - acetic acid mixture (75 mL) at 0 °C. The crude product was purified by column chromatography (silica gel, 50% CHCl₃-hexane) to yield the pure product as yellow oil. Yield: 89%; δ_H (600 MHz, CDCl₃, ppm): 7.08 (s, 2H), 6.88 (s, 2H), 6.89 (s, 2H), 2.77 (t, *J* = 7.8 Hz, 4H), 2.71 (t, *J* = 7.8 Hz, 4H), 1.68-1.54 (m, 8H), 1.42-1.28 (m, 24H), 0.88 (m, 12H); δ_C (150 MHz, CDCl₃): 140.23, 139.95, 135.62, 132.90, 132.70, 131.92, 130.67, 129.09, 126.07, 110.33, 31.66, 31.60, 30.54, 30.51, 29.39, 29.23, 29.21, 29.09, 22.62, 22.58, 14.08.

2.3.4. Synthesis of 3,3',3''',3''''-sextihexyl-2,5':2',5''-2'',2''':5''',2''''-septithiophene (5): Dibromo quinque-thiophene **4** (907 mg, 1.00 mmol, 1.0 equiv.), 3-hexylthiophene-2-boronic acid pinacol ester (617 mg, 2.10 mmol, 2.1 equiv.), 2M aq. K₂CO₃ (5 mL), Aliquat 336 (1 drop), Pd(PPh₃)₄ (57 mg, 0.05 mmol, 0.05 equiv.), and toluene (8 mL) were used. The crude product was purified using column chromatography (silica gel, hexane). Pure product was obtained as a brick red solid. Yield: 70%; δ_H (600 MHz, CDCl₃, ppm): 7.16 (d, *J* = 4.4 Hz, 2H), 7.10 (s, 2H), 6.97 (s, 2H), 6.94 (d, *J* = 4.2 Hz, 2H), 2.78 (m, 12H), 1.67 (m, 12H), 1.33 (m, 36H), 0.89 (m, 18H); δ_C (150 MHz, CDCl₃, ppm): 139.93, 139.82, 139.62, 135.78, 134.10, 133.99, 130.54, 130.33, 130.10, 128.75, 128.56, 125.91, 123.58, 31.68, 31.57, 31.67, 30.67, 30.60, 30.50, 29.28, 29.24, 29.21, 22.63, 14.10.

2.3.5. Synthesis of 5,5''''-diformyl-3,3',3''',3''''-sextihexyl-2,5':2',5''-2'',2''':5''',2''''-septithiophene (6): A Vilsmeier reagent was prepared by mixing POCl₃ (0.16 mL, 1.81 mmol, 3.01 equiv.) and DMF (0.66 mL, 9.0 mmol, 15.0 equiv.). In another two necked flask, septithiophene **5** (650 mg, 0.60 mmol, 1.0 equiv.) was dissolved in anhydrous 1,2-dichloroethane (7 mL) by stirring, and cooled to 0 °C using an ice bath under argon atmosphere. To this solution, the Vilsmeier reagent was added dropwise, the reaction mixture was then heated to 60 °C, and stirred for 12 h. The mixture was poured into ice water (200 mL), neutralized with Na₂CO₃, and then extracted with CH₂Cl₂. The combined organic layer was washed with brine, water, and dried over Na₂SO₄. After removal of solvent, the crude product was purified using column chromatography (silica gel, 70% CH₂Cl₂-hexane) to afford **6** as a brown solid. Yield: 80%; δ_H (600 MHz, CDCl₃, ppm): 9.82 (s, 2H), 7.58 (s, 2H), 7.25 (s, 2H), 7.14 (d, *J* = 3.6 Hz, 4H), 7.01 (s, 2H), 2.81 (m, 12H), 1.70 (m, 12H), 1.35 (m, 36H), 0.90 (m, 18H); δ_C (150 MHz, CDCl₃, ppm): 181.88, 141.21, 140.43, 140.34, 140.25, 140.06, 139.15, 135.82, 133.31, 132.79,

132.65, 130.94, 130.52, 129.23, 126.18, 31.90, 30.98, 30.81, 30.65, 30.46, 29.99, 29.64, 29.58, 29.52, 22.62, 14.11.

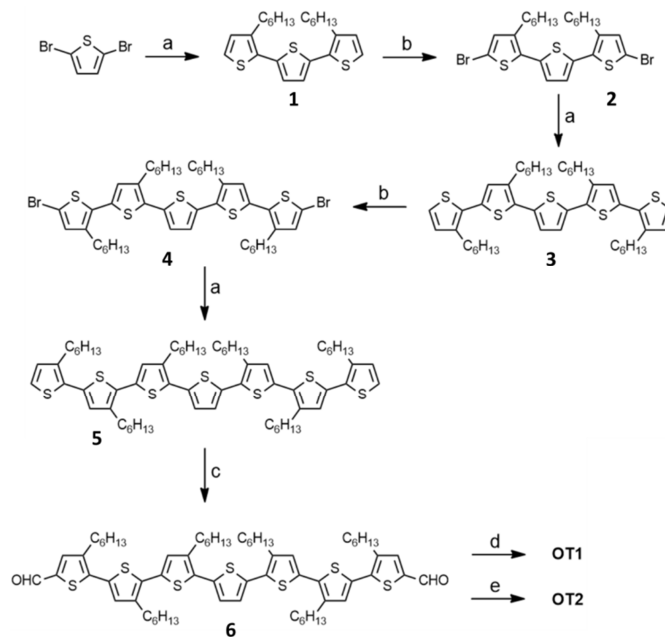
2.3.6. Synthesis of OT1: OT1 was prepared by dissolving diformylseptithiophene derivative **6** (50 mg, 0.04 mmol, 1 equiv.) and 2-phenyl-5-oxazolone (54 mg, 0.34 mmol, 8.0 equiv.) in dry chloroform (10 mL) by stirring under argon atmosphere. Three drops of triethylamine was added to the reaction mixture, stirred for 8 h at room temperature, and for 1 h at 60 °C. The reaction mixture was then diluted with CHCl₃, washed with water and brine. The combined organic layer was dried over Na₂SO₄, and evaporated to dryness under vacuum. The crude product was purified by column chromatography (silica gel, CHCl₃) to afford the OT1 as blackish brown solid. Yield: 88%; m.p: 193-194 °C. δ_{H} (500 MHz, CDCl₃, ppm): 8.20 (d, $J = 8$ Hz, 4H), 7.61 (t, $J = 8.4$ Hz, 2H), 7.55 (t, $J = 9$ Hz, 4H), 7.42 (s, 2H), 7.39 (s, 2H), 7.18 (s, 2H), 7.14 (s, 2H), 7.05 (s, 2H), 2.86-2.82 (m, 12H), 1.72 (d, $J = 6$ Hz, 12H), 1.45 (s, 12H), 1.36 (t, $J = 4.8$ Hz, 24H), 0.92 (t, $J = 3.6$ Hz, 18H); δ_{C} (125 MHz, CDCl₃): 167.01, 161.93, 141.32, 140.27, 138.85, 135.73, 135.00, 133.55, 133.01, 132.30, 130.79, 130.31, 128.91, 128.27, 126.09, 125.69, 124.58, 31.66, 30.49, 30.18, 30.11, 29.76, 29.68, 29.43, 29.22, 29.17, 22.63, 14.09; IR (KBr) ν_{max} : 2920, 2848, 1785, 1639, 1555, 1441, 1326, 1263, 1149, 1086, 1013, 815, 690, 576 cm⁻¹; MALDI-TOF-MS: $m/z = 1423.15$ (calcd = 1422.56).

2.3.7. Synthesis of OT2: OT2 was synthesized by following a similar procedure employed for preparing OT1 using diformylseptithiophene derivative **6** (50 mg, 0.04 mmol, 1.0 equiv.), 3-phenyl-5-isoxazolone (54 mg, 0.34 mmol, 8.0 equiv.), and dry chloroform (10 mL). The crude product was purified by column chromatography (silica gel, CHCl₃) to afford the OT2 as dark brown solid. Yield: 88%; m.p: 74-75 °C; δ_{H} (500 MHz, CDCl₃, ppm): δ 7.75 (s, 2H), 7.62-7.58 (m, 12H), 7.324 (s, 2H), 7.13 (s, 2H), 7.05 (2H), 2.86-2.80 (m, 12H), 1.74-1.68 (m, 12H), 1.42 (t, $J = 6$ Hz, 12H), 1.34 (m, 24H), 0.90 ppm (t, $J = 3.6$ Hz, 18H); δ_{C} (125 MHz, CDCl₃): 173.89, 164.93, 149.82, 143.18, 138.45, 138.13, 138.02, 137.11, 136.62, 133.13, 131.67, 131.05, 129.25, 128.77, 128.28, 126.17, 124.61, 31.65, 30.58, 30.52, 30.06, 29.70, 29.51, 29.37, 29.31, 29.22, 22.65, 14.12; IR (KBr) ν_{max} : 2924, 2846, 1789, 1635, 1545, 1429, 1324, 1262, 1147, 1095, 1022, 814, 689, 564 cm⁻¹; MALDI-TOF-MS = 1422.89 (calcd = 1422.56).

Results and discussion

Synthesis and characterization of oligothiophene derivatives

OT1 and OT2 were synthesized according to methods reported in literature as shown in Scheme 1. Suzuki coupling followed by dibromination reactions were employed successively to achieve thiophene oligomer with seven thiophene units. It was then functionalized with aldehyde groups at both ends by treating with Vilsmeier reagent. Incorporation of oxazolone/isoxazolone acceptors to the thiophene backbone was carried out by Knoevenagel condensation method. Both derivatives were obtained in good yields, and characterized by using various analytical techniques such as ¹H NMR, ¹³C NMR, IR and MALDI-TOF mass spectrometry. They were found to be soluble in common organic solvents such as toluene, CHCl₃, chlorobenzene, THF, DMF etc.



Scheme 2. Synthetic route for the preparation of OT1 and OT2. Reagents and conditions: (a) 3-hexylthiophene-2-boronic acid pinacol ester, 2M aq. K₂CO₃, Pd(PPh₃)₄, Aliquat 336, toluene, reflux, Ar, 24 h; (b) NBS, AcOH, CHCl₃; (c) POCl₃, DMF, 1,2-dichloroethane; (d) 2-Phenyl-5-oxazolone, NEt₃, dry CHCl₃, (e) 3-Phenyl-5-isoxazolone, NEt₃, dry CHCl₃.

Photophysical properties in solution state

Table 1. Photophysical parameters such as absorption maxima, emission maxima, extinction coefficients (ϵ) and fluorescence quantum yields (ϕ_{f}) of OT1 and OT2 in various solvents.

Compound	Solvent	Absorption		Emission		
		λ_{max} (nm)	$\epsilon \times 10^5$ (M ⁻¹ cm ⁻¹)	λ_{max} (nm)	ϕ_{f} (%) ^a	τ (ns)
OT1	Cyclohexane	487	0.35	614	52	0.90
	Toluene	504	0.34	643	33	0.88
	THF	496	0.35	700	15	0.74
	DMF	497	0.24	-	-	-
OT2	Cyclohexane	510	0.78	639	1.2	0.21
	Toluene	527	0.82	685	2.3	0.19
	THF	519	0.84	745	2.5	0.20
	DMF	529	0.78	-	-	-

^a Rhodamine B in ethanol ($\phi_{\text{f}} = 0.5$) was used as the standard for quantum yield measurement, error limit $\pm 5\%$.

The UV-vis absorption and fluorescence properties of OT1 and OT2 were studied in solvents such as cyclohexane, toluene, tetrahydrofuran (THF), and *N,N*-dimethylformamide (DMF) at a concentration of 1×10^{-5} M, and the details are summarized in Table 1. The solvent polarity increases from cyclohexane to DMF. In general, both molecules exhibited an intense broad absorption in the UV-visible region, which is typically observed for conjugated thiophene oligomers. The most intense

band observed in the visible region could be attributed to the π - π^* transition. Although the trend is not regular with the solvent polarity, the absorption maximum of both molecules was fairly sensitive to the solvent polarity indicating that the ground state of the molecules is slightly polarized. This could be attributed to the conjugation of electron donating thiophenes with electron withdrawing oxazolone/isoxazolone derivatives, resulting in the localization of electron cloud towards the latter. This was evident from the DFT results, which showed HOMO is localized on the thiophene backbone, whereas the LUMO is biased towards the oxazolone/isoxazolone acceptors (see supporting information, Figure S1). It should be noted that the absorption maximum of **OT2** is about 20 nm red-shifted, and the extinction coefficient is almost double in any solvent when compared to that of **OT1** in the same solvent. Both these observations indicate that the isoxazolone derivative is a stronger acceptor than the oxazolone derivative, leading to the red-shifted absorption peak of the latter.

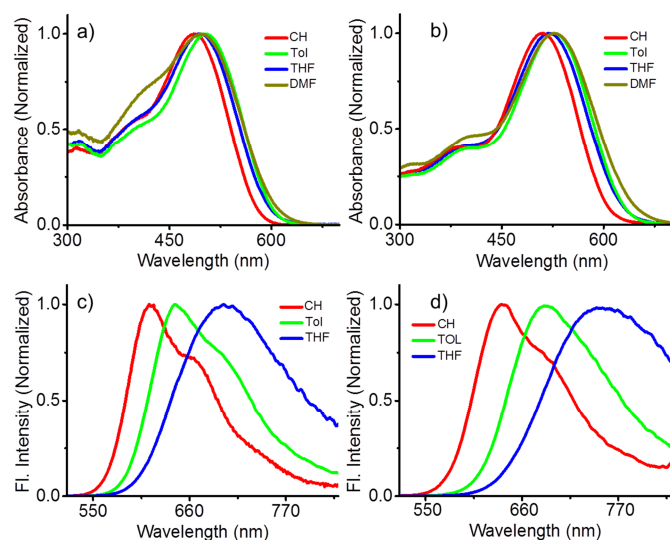


Fig. 1 UV-vis absorption spectra of (a) **OT1** and (b) **OT2**; fluorescence emission spectra of (c) **OT1** and (d) **OT2** in cyclohexane (CH), toluene (Tol), tetrahydrofuran (THF) and *N,N*-dimethylformamide (DMF; $c = 1 \times 10^{-5}$ M, $l = 1$ cm, $\lambda_{ex} = 490$ nm).

Emission spectra were also measured in cyclohexane, toluene, THF, and DMF. However, in contrast to absorption, fluorescence showed high sensitivity towards the solvent polarity, as evident from the significant red-shift of the emission maximum with increasing solvent polarity. This observation revealed that the excited states of both molecules are highly polar (compared to the ground state) in nature. Both molecules were found to be non-emissive in DMF, which is the highest polar solvent among the four. In the other three solvents, **OT1** exhibited good emission quantum yields, whereas **OT2** was poorly emissive. Similarly, the average fluorescence lifetime was higher for **OT1** than that of **OT2** (see supporting information, Figure S2). Similar to the absorption properties, **OT2** showed more red-shift than that of **OT1** in the same solvents. Moreover, **OT2** exhibited an emission maximum shift of 106 nm when going from cyclohexane to THF, whereas, **OT1** showed a shift of only 86 nm under similar conditions. These observations reiterate that isoxazolone derivative is a stronger acceptor than the oxazolone derivative. **OT1** showed the decrease in fluorescence quantum yield as

well as lifetime (negligible in the case of cyclohexane and toluene solutions) with increase in solvent polarity which is expected for donor-acceptor systems exhibiting charge transfer. However, such trends were not clear in **OT2** due to poor emission.

HOMO-LUMO levels and optical band-gap.

The HOMO levels of the oligomers were measured in film state as ionization threshold energy using ultraviolet photoelectron spectroscopy (PYS, Figure 2a, b). PYS measurements showed that the HOMO energy levels of **OT1** and **OT2** were at -5.09 and -5.32 eV, respectively. The LUMO levels were obtained by adding the value of HOMO to the optical band gap (E_g^{opt}), which is obtained from the onset of UV-vis absorption of the oligomers in the film state (details of film state absorption is given in the following section). The optical band gap of **OT1** and **OT2** was found to be 1.65 and 1.67 eV, respectively. Accordingly, the LUMO levels were found to be -3.44 and -3.65 eV for **OT1** and **OT2** respectively. The deeper HOMO and LUMO values for **OT2** reiterate better delocalization of π -electrons due to the presence of stronger electron withdrawing isoxazolone derivative in it. The comparison of HOMO and LUMO of the oligomers with that of P3HT (a standard donor material; HOMO = -4.9 eV, LUMO = -2.7 eV)⁴⁶ and PCBM (a standard acceptor material; HOMO = -6.0 eV, LUMO = -4.2 eV,¹⁰ where the latter is varied by the method and calibrating equation⁴⁷) is shown in Figure 2c. It shows that the HOMO and LUMO levels of the oligomers are lower than that of the corresponding energy levels of P3HT, whereas those are higher than that of the corresponding energy levels of PCBM. Further, the energy offset between the LUMOs of oligomers and P3HT/PCBM is high enough for exciton splitting at the interfaces. Hence, it could be assumed that both oligomers can act as a donor to PCBM and acceptor to P3HT in a photovoltaic cell.

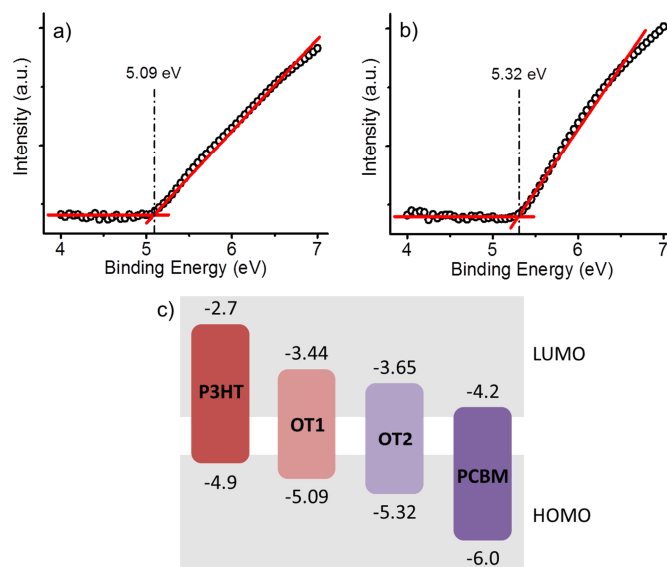


Fig. 2 PYS spectra of a) **OT1** and b) **OT2** in the film state. c) Scheme showing the comparison of the HOMO-LUMO levels of the oligomers with that of P3HT and PCBM.

Photovoltaic properties.

Though the electrochemical properties revealed that both **OT1** and **OT2** can act as a donor to PCBM and acceptor to P3HT, the p/n-polarity of a material in BHJ solar cells depends on not only the ability to donate/accept electrons but also the ability to transport holes/electrons. To check the p/n-polarity of **OT1** and **OT2** in a photovoltaic cell, bulk-heterojunction organic solar cells were fabricated in presence of P3HT or PCBM. An inverted device structure^{48,49} consisting of ITO/ZnO/BHJ/MoOx/Ag was used for this analysis. The active layer consists of **OT1**:P3HT, **OT1**:PCBM, **OT2**:P3HT, or **OT2**:PCBM in 1:1 weight ratio was prepared from chlorobenzene solution. **OT1**:P3HT solar cell showed a power conversion efficiency (PCE) of only 0.07 % (short circuit current density: $J_{SC} = 0.69$ mA/cm², open circuit voltage: $V_{OC} = 0.36$ V, fill factor: $FF = 0.28$, Figure S3). On the other hand, **OT1**:PCBM cell exhibited the PCE of 0.75 % ($J_{SC} = 3.25$ mA/cm², $V_{OC} = 0.62$ V, $FF = 0.37$). Under identical conditions, **OT2**:P3HT exhibited an efficiency of 0.19 % ($J_{SC} = 0.72$ mA/cm², $V_{OC} = 0.71$ V, $FF = 0.36$), whereas **OT2**:PCBM exhibited no diode characteristics. *J-V* curves of the **OT1**:PCBM and **OT2**:P3HT cells are shown in Figure 3a and 3b respectively. The atomic force microscopy images of the corresponding films were shown in the insets.

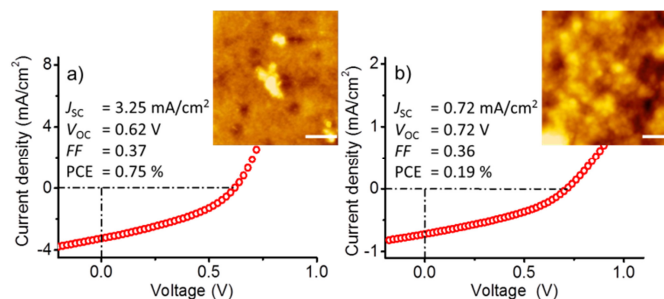


Fig. 3 *J-V* characteristics of photovoltaic devices fabricated from a solution of a) **OT1**:PCBM and b) **OT2**:P3HT (1:1 blend) in chlorobenzene (device structure: glass/ITO/ZnO/BHJ/MoOx/Ag). AFM height images of the corresponding active layers shown in the inset (scale bar corresponds to 500 nm).

Though the oligomers showed relatively low photoconversion efficiencies, the observed difference in the p/n-polarity of **OT1** and **OT2** in the presence of P3HT/PCBM was noteworthy. It is clear that **OT1** has showed more p-type characteristics, whereas **OT2** exhibited n-type characteristics. This could be partially explained by the difference in the relative HOMO-LUMO levels of the molecules. The shallower HOMO and LUMO of **OT1** (compared to **OT2**) provide better driving force for it to donate electrons and make it functioning as a donor. Similarly, deeper HOMO and LUMO of **OT2** is suitable for accepting electrons and make it functioning as an acceptor. The play of energy offset difference between the oligomers is particularly visible when they are blended with P3HT. i.e., **OT2**, which is having the higher energy offset showed better photoconversion efficiency than that of **OT1**. However, such logics could not explain the observed difference in photoconversion efficiency when the oligomers are blended with PCBM. **OT1** showed an efficiency of 0.75% in presence of PCBM, whereas **OT2** exhibited no diode characteristics under identical conditions.

Energy minimized structure

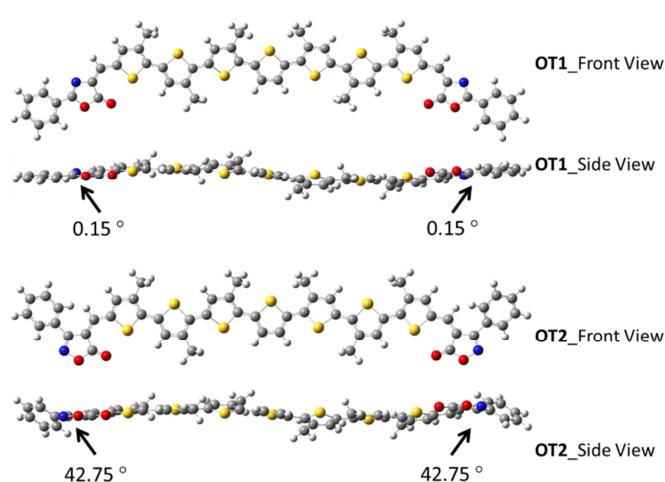


Fig. 4 Energy minimized structures of the oligomers obtained by DFT calculation.

It is well known that the supramolecular interactions and packing of the molecules in the film state plays a very important role on the charge carrier generation, charge carrier transport and photovoltaic properties.^{41,42,50-53} Planarity of the conjugated backbone is a key factor that decides the packing ability of conjugated oligomers. In order to get an insight into the planarity of the molecules, the energy minimized structures of the oligomers were calculated using density functional theory (DFT) at the B3LYP/6-31G(d,p) level (Figure 4). The conjugated thiophene backbones of both molecules looked similar, and were relatively planar. The major difference between the molecules was seen at the ends. The oxazolone derivative of **OT1** was found to be coplanar with the thiophene backbone, whereas, the phenyl group on the isoxazolone derivative in **OT2** was found to be out of plane. The dihedral angle between the isoxazolone and the attached phenyl ring in **OT2** was about 42.75°. The out of plane geometry of the phenyl ring in **OT2** could have a detrimental effect on the packing of the oligomers in the film state.

Film state absorption properties

The steady state photoabsorption spectra of both oligomers were taken in the film state by spin-casting from chlorobenzene (1 wt%) solution. For comparison, the corresponding absorption in the solution state in chlorobenzene was also recorded. **OT1** in chlorobenzene solution exhibits an absorption maximum at 513 nm, which was red-shifted to 621 nm in the film state. On the other hand, absorption maximum of **OT2** was at 540 nm in solution state and 609 nm in the film state. As explained in previous section, relative red-shift of the absorption maximum for **OT1** than that of **OT2** in same solvents could be attributed to the better electron accepting ability of isoxazolone derivative. The red-shift exhibited by both molecules when going from solution to film state indicates the planarization of the conjugated backbone. However, **OT1** and **OT2** exhibited a significant difference in this aspect; the relative red-shift was higher for **OT1** ($\Delta\lambda = 108$ nm) when compared to that of **OT2** ($\Delta\lambda = 69$ nm). Moreover, an additional shoulder band also appeared for **OT1** at around 683 nm, which is absent in the case of **OT2**. These observations correlates well with the results obtained from DFT calculations.

OT1 with coplanar oxazolone acceptor is able to form highly ordered aggregates through supramolecular interactions, mainly π - π stacking, which is evident from the vibronic shoulder seen at 683 nm. Such ordering further improves the planarity of the conjugated backbone and electronic communication between the molecules leading to the significant red-shift in film state. On the other hand, **OT2** with out-of-plane isoxazolone acceptor is unable to form well-ordered aggregates because of weaker π - π stacking, which is reflected from the absence of vibronic features as well as a lesser red-shift in the film state absorption.

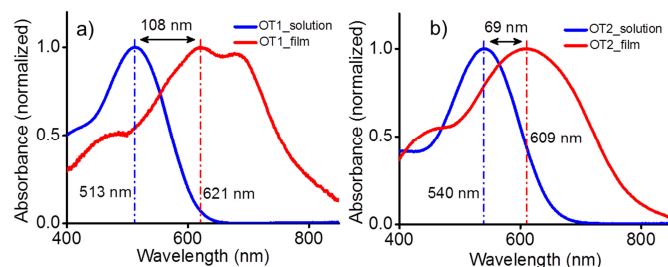


Fig. 5 Normalized absorption spectra of a) **OT1** and b) **OT2** in chlorobenzene solution (blue line, $c = 1 \times 10^{-5}$ M, $l = 1$ cm) and in film state (red line, spin-cast from 1 wt% chlorobenzene solution).

Solid state packing and thermal stability

In order to get a better insight into the supramolecular packing, we have carried out wide-angle X-ray scattering (WAXS) studies in the self-assembled powder state. **OT1** showed sharp and intense WAXS peaks, which indicates that the molecules are relatively ordered in the aggregated state. The sharp reflection at $2\theta = 5.42^\circ$ corresponds to 16.3 Å, which is well correlated with the lamellar distance. The mean size of the **OT1** crystallites was estimated as 21 nm using Scherrer's relation.⁵⁴ On the other hand, **OT2** exhibited less intense and broad peaks, particularly in the higher angle region (corresponding to intermolecular stacking distances). The reflection at $2\theta = 5.86^\circ$ corresponds to 15.1 Å, which is slightly lower than the lamellar distance. The intensity of this peak is six fold less when compared to that of the corresponding peak of **OT1**. Since the integrated intensity is directly proportional to the volume of nanodomains, consequently, the crystallinity of **OT2** is less than **OT1**. Hence it could be confirmed that the positional isomerism exhibited by the acceptors significantly affects the supramolecular interactions, which is reflected in the bulk packing. Relatively disordered packing in **OT2** may provide higher free volume for the alkyl chains thus reducing the spacing between the oligomers through slight intercalation of the alkyl chains. The thermal stability of the molecules was investigated by thermogravimetric analysis (TGA), which was conducted with a heating rate of $10^\circ\text{C min}^{-1}$ in the presence of nitrogen. The temperature at which **OT1** loses 5% of its weight (T_5 value) was 348°C while that of **OT2** was at 261°C . Comparison of the T_5 values of the **OT1** and **OT2** reveals that the **OT1** is thermally more stable than **OT2**, which reiterates the higher crystallinity in the former. Based on these observations, the supramolecular packing in the oligomers could be schematically represented as shown in Figure 7.

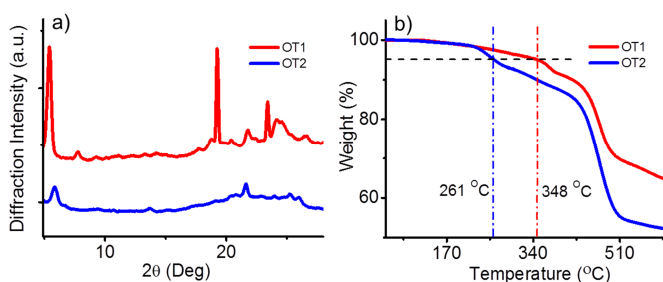


Fig. 6 a) X-ray diffraction patterns of **OT1** and **OT2** in the self-assembled powder state. b) TGA profiles of **OT1** and **OT2**; the black line indicates the temperatures at which the material loses 5% of its initial weight.

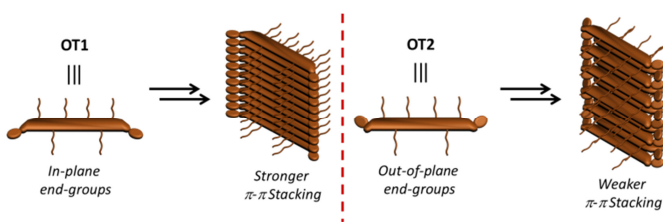


Fig. 7 Simplified schematic representation of the supramolecular organization of **OT1** and **OT2** in the self-assembled state.

Blend with P3HT and PCBM

In an attempt to study the effect of PCBM and P3HT on the film state packing of **OT1** and **OT2**, 1:1 (w/w) mixture of these compounds with PCBM/P3HT were prepared in chlorobenzene and the photoabsorbance of the blend films were recorded. The absorption maximum (λ_{max}) of **OT1**/P3HT blend film was observed at 606 nm while that of **OT1**/PCBM was at 612 nm. It should be noted that the vibronic features of the **OT1** absorption were intact even in the blend state which indicates that the supramolecular interactions in **OT1** is strong enough and remain stable on addition of P3HT or PCBM. Film state absorbance of **OT2** with P3HT and PCBM were measured under identical conditions. The absorption maximum of **OT2**/P3HT blend film was at 607 nm, while that of **OT2**/PCBM was at 563 nm. It could be assumed that the spherically shaped PCBM completely destroys the packing in **OT2** resulting in the blue-shift of the absorption maximum by 48 nm when compared to the pristine film. This further proves that the supramolecular interactions in **OT2** are weaker. However, no such blue-shift was observed on addition of P3HT, but some vibrational features were observed between 500 – 700 nm in the spectrum. The vibrational features could be attributed to the crystallite formation of P3HT,⁵⁵ which may not interfere with the stacking of **OT2**. In other words, **OT2** molecules might be pushed away during the P3HT crystallites formed during the film development process, resulting in the pure **OT2** domains.

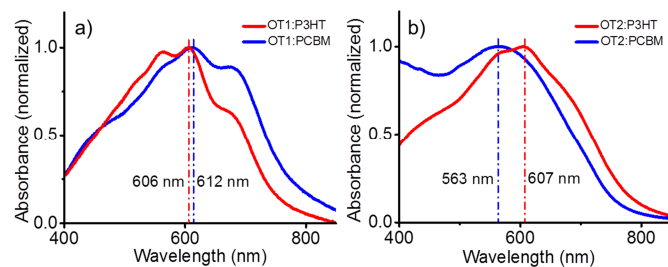


Fig. 8 Normalized absorption spectra of a) **OT1** and b) **OT2** blend films (1:1 w/w) with P3HT and PCBM spin-cast from chlorobenzene solution.

Photoconductivity Analysis

Photoconductivity measurements using flash-photolysis time-resolved microwave conductivity (FP-TRMC) is an excellent method to understand the charge carrier generation and transport dynamics of organic semiconducting materials.^{41,42,50-53,56} FP-TRMC is an electrode-less technique, which gives information about the short-range (nanometer scale) intrinsic charge carrier transport property, which could be quantified in terms of $\phi\Sigma\mu$ values where ϕ is the charge carrier generation quantum yield on excitation with laser light and $\Sigma\mu$ is the sum of charge carrier mobilities, i.e., the sum of electron and hole mobilities (μ_e and μ_h , respectively). Photoconductivity transients obtained from FP-TRMC usually reflect the molecular as well as supramolecular properties, and hence helpful for correlating the structure, property, and device performance relationship.^{13,28,42,50,51} The photoconductivity transients of **OT1** and **OT2**, and their blends with P3HT and PCBM in film state is shown in Figure 9. Both **OT1** and **OT2** exhibited comparable values of $\phi\Sigma\mu_{\max}$ ($1.4 \times 10^{-5} \text{ cm}^2 \text{ V}^{-1} \text{ s}^{-1}$ and $1.7 \times 10^{-5} \text{ cm}^2 \text{ V}^{-1} \text{ s}^{-1}$ respectively) on excitation with 500 nm laser. $\phi\Sigma\mu_{\max}$ of **OT1** showed a 5 fold enhancement in presence of P3HT (1:1 w/w) and a 24 fold increase in the presence of PCBM (1:1 w/w). This is consistent with the J_{sc} of the relevant OPV devices (**OT1**:P3HT – 0.69 mA/cm² and **OT1**:PCBM – 3.25 mA/cm²). Significant enhancement of the photoconductivity in the presence of PCBM reiterated the p-type characteristics of **OT1**. On the other hand, under identical conditions, $\phi\Sigma\mu_{\max}$ of **OT2** increased by only 4 times in the presence of PCBM, and that of 25 times on the addition of P3HT. This gave further proof for the n-type characteristics of **OT2**. We emphasize again that the FP-TRMC results are in line with the OPV devices (**OT2**:PCBM showed no diode output and **OT2**:P3HT – 0.72 mA/cm²).

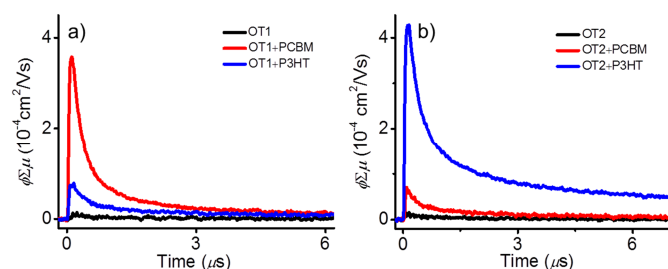


Fig. 9 TRMC transients of **OT1** and **OT2** films and their blends (1:1 w/w) with PCBM and P3HT drop-cast from chlorobenzene solution.

From the above studies, it is evident that the observed p/n-polarity of **OT1** and **OT2** in the bulk heterojunction assembly with P3HT/PCBM could be correlated to their molecular as well as supramolecular properties. The n-polarity of the molecules in presence of P3HT could be mainly correlated to the relative HOMO-LUMO levels, which is a molecular property. However, the supramolecular effect is not completely ruled out either. In the presence of crystalline polymeric materials such as P3HT, amorphous **OT2** has an advantage over crystalline **OT1** due to effective nanoscale miscibility. This effect might help the former to perform well in the presence of P3HT. On the other hand, the p-polarity exhibited by the molecules could be exclusively dependent on the supramolecular interactions. **OT1** with a planar geometry formed stable assembly, whereas, **OT2** containing non-planar end-groups formed weak assembly. As a result, the former assembly remained stable on addition of spherically shaped PCBM and functioned as an efficient p-type material in the presence of PCBM. On the other hand, **OT2** got dis-assembled in the presence of PCBM, and hence failed to function as a p-type material.

Though these molecules illustrate an interesting example for the effect of molecular structure on the supramolecular properties and thereby their p/n-polarity in bulk-heterojunction solar cells, the device performance fell short of expectation. This could be mainly attributed to the low value of J_{sc} , probably due to the lack of continuity in the oligomer phase resulting in hindered charge transport. As mentioned earlier, unlike polymers, oligomers are exclusively depends on the intermolecular route for charge transport. Lack of continuity is detrimental to efficient charge carrier transport to the electrodes and results poor device performances. This may also results in imbalanced charge carrier mobility and lowers the FF value.

Conclusions

In summary, two thiophene oligomers with acceptor-donor-acceptor structure consisting of oxazolone/isoxazolone derivatives as acceptors have been designed and synthesized. Isoxazolone derivative (**OT2**) was found to be a stronger electron-withdrawing unit than that of oxazolone derivative (**OT1**), as evident from the photoabsorption and emission spectroscopy. Importantly, we have showed that the positional isomerism had a significant effect on the supramolecular properties. The suitable HOMO-LUMO energy levels of **OT2** favored it to act as a better n-type material in presence of P3HT in bulk-heterojunction solar cells. On the other hand, better supramolecular interaction in **OT1** helped it to form stable bicontinuous network with PCBM, and hence acted as a p-type material, which is consistent with the FP-TRMC evaluations. Though the importance of molecular and supramolecular properties on device performances is well established, this work clearly illustrates how delicate changes on basic molecular structure affect the ordering and p/n-polarity of organic semiconducting materials in bulk-heterojunction photovoltaic cells.

Acknowledgements

This work was financially supported by DST through Ramanujan Fellowship (SR/S2/RJN-133/2012). T.G. is grateful to CSIR for Junior Research Fellowship. The authors thank Dr. Bhoje Gowd for XRD measurement, Mr. Peer Mohamed for TGA and Kiran J. S. for artwork.

Notes and references

^a Photosciences and Photonics Section, CSIR-National Institute for Interdisciplinary Science and Technology (NIIST), Trivandrum 695 019, India.

^b Department of Applied Chemistry, Graduate School of Engineering, Osaka University, 2-1 Yamadaoka, Suita, Osaka 565-0871, Japan here.

^c Academy of Scientific and Innovative Research (AcSIR), New Delhi 110 001, India.

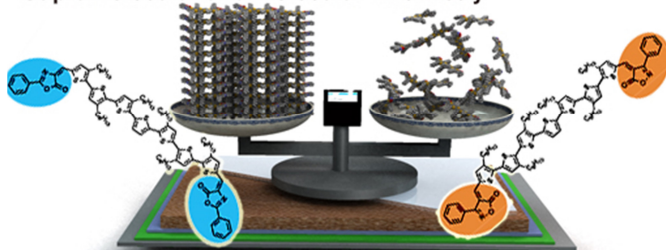
† Electronic Supplementary Information (ESI) available: Figures showing HOMO and LUMO distribution of the oligomers calculated by DFT method, the fluorescence lifetime decay of **OT1** and **OT2** in various solvents, and *J-V* characteristics of **OT1**:P3HT (1:1 blend) BHJ device with the corresponding AFM height image of the active layer. See DOI: 10.1039/b000000x/

- J.-S. Wu, S.-W. Cheng, Y.-J. Cheng and C.-S. Hsu, *Chem. Soc. Rev.*, 2015, (DOI: 10.1039/C4CS00250D).
- J. Subbiah, B. Purushothaman, M. Chen, T. Qin, M. Gao, D. Vak, F. H. Scholes, X. Chen, S. E. Watkins, G. J. Wilson, A. B. Holmes, W. W. H. Wong and D. J. Jones, *Adv. Mater.*, 2015, **27**, 702–705.
- K. Li, Z. Li, K. Feng, X. Xu, L. Wang and Q. Peng, *J. Am. Chem. Soc.*, 2013, **135**, 13549–13557.
- M. Kaltenbrunner, M. S. White, E. D. Głowacki, T. Sekitani, T. Someya, N. S. Sariciftci and S. Bauer, *Nat. Commun.*, 2012, **3**, 770.
- D. Angmo, T. T. Larsen-olsen and F. C. Krebs, *Mater Today*, 2012, **15**, 36–49.
- Y. Huang, E. J. Kramer, A. J. Heeger and G. C. Bazan, *Chem. Rev.*, 2014, **114**, 7006–7043.
- D. Amarasinghe Vithanage, a Devižis, V. Abramavičius, Y. Infahsaeng, D. Abramavičius, R. C. I. MacKenzie, P. E. Keivanidis, a Yartsev, D. Hertel, J. Nelson, V. Sundström and V. Gulbinas, *Nat. Commun.*, 2013, **4**, 2334.
- G. Yu, J. Gao, J. C. Hummelen, F. Wudl and A. J. Heeger, *Science* 1995, **270**, 1789–1791.
- F. Martini, S. Borsacchi, S. Spera, C. Carbonera, A. Cominetti and M. Geppi, *J. Phys. Chem. C*, 2013, **117**, 131–139.
- B. C. Thompson and J. M. J. Fréchet, *Angew. Chem. Int. Ed. Engl.*, 2008, **47**, 58–77.
- Y. Kim, S. Cook, S. M. Tuladhar, S. a. Choulis, J. Nelson, J. R. Durrant, D. D. C. Bradley, M. Giles, I. McCulloch, C.-S. Ha and M. Ree, *Nat. Mater.*, 2006, **5**, 197–203.
- J. L. Segura, N. Martin and D. M. Guldi, *Chem. Soc. Rev.*, 2005, **34**, 31–47.
- B. Balan, C. Vijayakumar, A. Saeki, Y. Koizumi, M. Tsuji and S. Seki, *Polym. Chem.*, 2013, **4**, 2293–2303.
- Y. Koizumi, M. Ide, A. Saeki, C. Vijayakumar, B. Balan, M. Kawamoto and S. Seki, *Polym. Chem.*, 2013, **4**, 484–494.
- C. Vijayakumar, A. Saeki and S. Seki, *Chem. Asian J.*, 2012, **7**, 1845–1852.
- H. Zhou, L. Yang and W. You, *Macromolecules*, 2012, **45**, 607–632.
- Y.-J. Cheng, S.-H. Yang and C.-S. Hsu, *Chem. Rev.*, 2009, **109**, 5868–923.
- K. R. Graham, C. Cabanetos, J. P. Jahnke, M. N. Idso, A. El Labban, G. O. N. Ndjawa, T. Heumueller, K. Vandewal, A. Salleo, B. F. Chmelka, A. Amassian, P. M. Beaujuge and M. D. McGehee, *J. Am. Chem. Soc.*, 2014, **136**, 9608–9618.
- F. Li, K. G. Yager, N. M. Dawson, Y. Jiang, K. J. Malloy and Y. Qin, *Chem. Mater.*, 2014, **26**, 3747–3756.
- K. Yao, L. Chen, F. Li, P. Wang and Y. Chen, *J. Phys. Chem. C*, 2012, **116**, 714–721.
- G. Li, V. Shrotriya, J. Huang, Y. Yao, T. Moriarty, K. Emery, Y. Yang, *Nat. Mater.* **2005**, **4**, 864–868.
- L. Chang, H. W. a. Lademann, J.-B. Bonekamp, K. Meerholz and A. J. Moulé, *Adv. Funct. Mater.*, 2011, **21**, 1779–1787.
- D. H. Wang, P.-O. Morin, C.-L. Lee, A. K. Ko Kyaw, M. Leclerc and A. J. Heeger, *J. Mater. Chem. A*, 2014, **2**, 15052–15057.
- K. R. Graham, J. Mei, R. Stalder, J. W. Shim, H. Cheun, F. Ste, F. So, B. Kippelen and J. R. Reynolds, *ACS Appl. Mater. Interfaces*, 2011, **3**, 1210–1215.
- J. S. Moon, C. J. Takacs, S. Cho, R. C. Coffin, H. Kim, G. C. Bazan and A. J. Heeger, *Nano Lett.*, 2010, **10**, 4005–4008.
- A. L. Ayzner, D. D. Wanger, C. J. Tassone, S. H. Tolbert and B. J. Schwartz, *J. Phys. Chem. C*, 2008, **112**, 18711–18716.
- E. Verploegen, R. Mondal, C. J. Bettinger, S. Sok, M. F. Toney and Z. Bao, *Adv. Funct. Mater.*, 2010, **20**, 3519–3529.
- B. Balan, C. Vijayakumar, A. Saeki, Y. Koizumi and S. Seki, *Macromolecules*, 2012, **45**, 2709–2719.
- C. Vijayakumar, B. Balan, A. Saeki, T. Tsuda, S. Kuwabata and S. Seki, *J. Phys. Chem. C*, 2012, **116**, 17343–17350.
- J. Zhou, Y. Zuo, X. Wan, G. Long, Q. Zhang, W. Ni, Y. Liu, Z. Li, G. He, C. Li, B. Kan, M. Li and Y. Chen, *J. Am. Chem. Soc.*, 2013, **135**, 8484–8487.
- S. Paek, H. Choi, J. Sim, K. Song, J. K. Lee and J. Ko, *J. Phys. Chem. C*, 2014, **118**, 27193–27200.
- Y. Lin, Y. Li and X. Zhan, *Chem. Soc. Rev.*, 2012, **41**, 4245–4272.
- A. Mishra and P. Bäuerle, *Angew. Chem. Int. Ed. Engl.*, 2012, **51**, 2020–2067.
- Y. Sun, G. C. Welch, W. L. Leong, C. J. Takacs, G. C. Bazan and A. J. Heeger, *Nat. Mater.*, 2012, **11**, 44–48.
- F. Zhang, D. Wu, Y. Xu and X. Feng, *J. Mater. Chem.*, 2011, **21**, 17590–17600.
- Q. Zhang, B. Kan, F. Liu, G. Long, X. Wan, X. Chen, Y. Zuo, W. Ni, H. Zhang, M. Li, Z. Hu, F. Huang, Y. Cao, Z. Liang, M. Zhang, T. P. Russell and Y. Chen, *Nat. Photonics*, 2014, **9**, 35–41.
- B. Kan, Q. Zhang, M. Li, X. Wan, W. Ni, G. Long, Y. Wang, X. Yang, H. Feng and Y. Chen, *J. Am. Chem. Soc.*, 2014, **136**, 15529–15532.
- Y. Liu, C.-C. Chen, Z. Hong, J. Gao, Y. M. Yang, H. Zhou, L. Dou, G. Li and Y. Yang, *Sci. Rep.*, 2013, **3**, 3356.
- P. Carbone and A. Troisi, *J. Phys. Chem. C*, 2014, **5**, 2637–2641.
- R. Noriega, J. Rivnay, K. Vandewal, F. P. V. Koch, N. Stingelin, P. Smith, M. F. Toney and A. Salleo, *Nat. Mater.*, 2013, **12**, 1038–1044.
- S. Yagai, Y. Goto, X. Lin, T. Karatsu, A. Kitamura, D. Kuzuhara, H. Yamada, Y. Kikkawa, A. Saeki and S. Seki, *Angew. Chem. Int. Ed.*, **2012**, **51**, 6643–6647.
- X. Lin, Y. Tani, R. Kanda, K.-i. Nakayama and S. Yagai, *J. Mater. Chem. A*, **2013**, **1**, 14686–14691.
- Gaussian 09, Revision A02, M. J. Frisch et. al., Gaussian Inc., Wallingford CT, 2009.
- A. Saeki, S. Seki, T. Sunagawa, K. Ushida and S. Tagawa, *Philos. Mag.*, 2006, **86**, 1261–1276.

45. Y. Liu, J. Zhou, X. Wan and Y. Chen, *Tetrahedron*, 2009, **65**, 5209–5215.
46. L.-L. Chua, J. Zaumseil, J.-F. Chang, E. C.-W. Ou, P. K.-H. Ho, H. Sirringhaus and R. H. Friend, *Nature*, 2005, **434**, 194–199.
47. B. W. Larson, J. B. Whitaker, X. Wang, A. a Popov, G. Rumbles, N. Kopidakis, S. H. Strauss and O. V Boltalina, *J. Phys. Chem. C*, 2013, **117**, 14958–14964.
48. J. J. Intemann, K. Yao, Y.-X. Li, H.-L. Yip, Y.-X. Xu, P.-W. Liang, C.-C. Chueh, F.-Z. Ding, X. Yang, X. Li, Y. Chen and A. K.-Y. Jen, *Adv. Funct. Mater.*, 2014, **24**, 1465–1473.
49. J. Sun, Y. Zhu, X. Xu, L. Lan, L. Zhang, P. Cai and J. Chen, *J. Phys. Chem. C*, 2012, **116**, 14188 –14198.
50. S. Prasanthkumar, S. Ghosh, V. C. Nair, A. Saeki, S. Seki and A. Ajayaghosh, *Angew. Chemie Int. Ed.*, 2015, **54**, 946–950.
51. M. Tsuji, A. Saeki, Y. Koizumi, N. Matsuyama, C. Vijayakumar and S. Seki, *Adv. Funct. Mater.*, 2014, **24**, 28–36.
52. A. Saeki, S. Yoshikawa, M. Tsuji, Y. Koizumi, M. Ide, C. Vijayakumar and S. Seki, *J. Am. Chem. Soc.*, 2012, **134**, 19035–19042.
53. A. Saeki, Y. Koizumi, T. Aida and S. H. U. Seki, *Acc. Chem. Res.* 2012, **45**, 1193–1202.
54. T. Erb, U. Zhokhavets, G. Gobsch, S. Raleva, B. Stühn, P. Schilinsky, C. Waldauf and C. J. Brabec, *Adv. Funct. Mater.*, 2005, **15**, 1193–1196.
55. S. D. Dimitrov and J. R. Durrant, *Chem. Mater.*, 2014, **26**, 616–630.
56. S. Prasanthkumar, A Seki, S. Seki and A. Ajayaghosh, *J. Am. Chem. Soc.*, 2010, **132**, 8866–8867.

Table of Content

Supramolecular and Molecular Chemistry



Effect of molecular and supramolecular properties on the p/n-polarity of two thiophene oligomers in bulk heterojunction solar cells are described.